1,2-Carbastanna-*closo*-dodecaborate, a New Tin Ligand in Coordination Chemistry: Synthesis, Structure, and Reactivity

Dominik Joosten,† Ines Weissinger,† Marius Kirchmann,† Cäcilia Maichle-Mössmer,† Falko M. Schappacher,‡ Rainer Pöttgen,‡ and Lars Wesemann*,†

Institut für Anorganische Chemie, Universität Tübingen, Auf der Morgenstelle 18, D-72076 Tübingen, Germany, and Institut für Anorganische und Analytische Chemie, Universität Münster, Corrensstrasse 30, D-48149 Münster, Germany

Received July 13, 2007

The synthesis of $[MePPh_3][SnCB_{10}H_{11}]$ is presented together with its structural, NMR, and ^{119}Sn Mössbauer spectroscopical characterization. Two transition metal complexes, $[Au_4(PPh_3)_4(SnCB_{10}H_{11})_2]$ and $[Bu_4N]_2[Rh(PPh_3)_2(SnCB_{10}H_{11})_3]$, with the carbastannaborate coordinated at rhodium or gold via the tin atom are presented, and the structural and NMR spectroscopical data are discussed.

Introduction

Whereas the group XIV heteroborate $[CB_{11}H_{12}]^-$ is well known for its properties as a weakly coordinating anion,[1−4] its heavier analogue, the stannaborate $[SnB_{11}H_{11}]^{2-}$, on the other hand, is a versatile ligand in coordination chemistry. The synthesis of $[SnB_{11}H_{11}]^{2-}$ was first described by Todd et al. in 1992 together with the homologous germanium and lead derivatives.[5] One striking feature is the stability of the dianion $[SnB_{11}H_{11}]^{2-}$ together with its nucleophilicity at the tin vertex, which led to a large number of transition metal coordination compounds prepared in our group during the last years.[6]

In contrast to the distinctive nucleophilic behavior of $[SnB_{11}H_{11}]^{2-}$, neutral cluster species containing tin and carbon, such as the *closo*-carbastannaboranes $Sn(CR)_2B_4H_4$,[7] $Sn(CMe)_2B_9H_9$,[8] and $Sn(CR_2)_2B_{10}H_{10}$,[9,10] show exclusively electrophilic character, which is manifested in the reaction with Lewis bases (e.g., PPh_3, THF, 2,2′-bipyridine) to form heteroborane cages with slipped tin vertices.[7]

In this article we present the synthesis of 1,2-carbastanna-*closo*-dodecaborate $[SnCB_{10}H_{11}]^-$, **1**, which might be the missing link between the nucleophilic $[SnB_{11}H_{11}]^{2-}$ and the electrophilic $[SnC_2B_9H_{11}]$ (Figure 1). Our main interest is to compare this new cluster molecule **1** with the Lewis basic $[SnB_{11}H_{11}]^{2-}$ and the Lewis acidic $[SnC_2B_9H_{11}]$ in terms of reaction behavior against nucleophiles and electrophiles. These efforts led to two new coordination compounds of the carbastannaborate, which are introduced here as well.

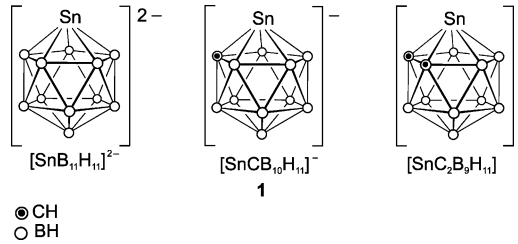

Figure 1. Sequence of tin-containing cluster species $[SnB_{11}H_{11}]^{2-}$, $[SnCB_{10}H_{11}]^-$ (**1**), and $[SnC_2B_9H_{11}]$.

Results and Discussion

Synthesis. The strategy for the preparation of $[SnCB_{10}H_{11}]^-$ is comparable to the synthesis of $[SnB_{11}H_{11}]^{2-}$ and $[SnC_2B_9H_{11}]$, where the *nido*-cages $[B_{11}H_{14}]^-$ and $[C_2B_9H_{12}]^-$, respectively, are used to form the tin-containing *closo*-clusters in the course of a typical salt elimination reaction with $SnCl_2$.[5,11] In analogy, the starting material for the preparation of **1** is the *nido*-carbaborate $[CB_{10}H_{13}]^-$, which is easily formed from the zwitterionic species $Me_3NCB_{10}H_{13}$ by reduction with sodium metal.[12]

The bridging hydrogen atoms of the open five-membered face are removed by *n*-butyllithium in THF, resulting in the formation of a colorless precipitate. On addition of $SnCl_2$ dissolved in THF, the mixture becomes clear again due to the formation of the monoanion $[SnCB_{10}H_{11}]^-$ (eq 1). This carbastannaborate can

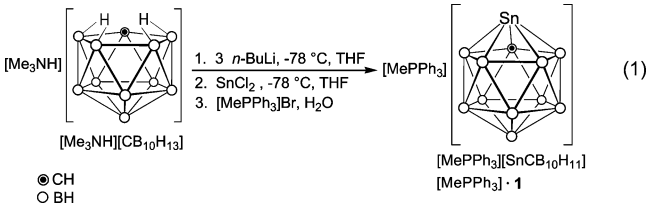

(1)

be precipitated from aqueous solution by a wide range of ammonium or phosphonium cations, e.g., $[Bu_4N]^+$, $[Bu_3NH]^+$, and $[MePPh_3]^+$. The resulting colorless solids are not sensitive toward moisture and can be stored under an inert atmosphere for months. The $[MePPh_3]^+$ salt was used for elemental analysis,

* Corresponding author. E-mail: lars.wesemann@uni-tuebingen.de.
† Universität Tübingen.
‡ Universität Münster.

(1) Reed, C. A. *Acc. Chem. Res.* **1998**, *31*, 133−139.
(2) Reed, C. A. *Chem. Commun.* **2005**, 1669−1677.
(3) Kim, K. C.; Reed, C. A.; Elliott, D. W.; Mueller, L. J.; Tham, F.; Lin, L.; Lambert, J. B. *Science* **2002**, *297*, 825−827.
(4) Müller, T.; Juhasz, M.; Reed, C. A. *Angew. Chem.* **2004**, *116*, 1569−1572; *Angew. Chem., Int. Ed.* **2004**, *43*, 1543−1546.
(5) Chapman, R. W.; Kester, J. G.; Folting, K.; Streib, W. E.; Todd, L. J. *Inorg. Chem.* **1992**, *31*, 979−983.
(6) Gädt, T.; Wesemann, L. *Organometallics* **2007**, *26*, 2474−2481.
(7) Saxena, A. K.; Maguire, J. A.; Hosmane, N. S. *Chem. Rev.* **1997**, *97*, 2421−2461.
(8) Jutzi, P.; Galow, P.; Abu-Orabi, S.; Arif, A. M.; Cowley, A. H.; Norman, N. C. *Organometallics* **1987**, *6*, 1024−1031.
(9) Wilson, N. M. M.; Ellis, D.; Boyd, A. S. F.; Giles, B. T.; MacGregor, S. A.; Rosair, G. M.; Welch, A. J. *Chem. Commun.* **2002**, 464−465.
(10) Wong, K. H.; Chan, H. S.; Xie, Z. *Organometallics* **2003**, *22*, 1775−1778.
(11) Rudolph, R. W. *Inorg. Chem.* **1974**, *13*, 248.
(12) Knoth, W. H.; Little, J. L.; Lawrence, J. R.; Scholer, F. R.; Todd, L. J. *Inorg. Synth.* **1968**, *11*, 33−41.

10.1021/om7006858 CCC: $37.00
Publication on Web 10/03/2007

the $[Bu_4N]^+$ salt shows good solubility in common solvents and therefore was used for the reactions with the transition metals, whereas the crystallization efforts yielded the best results with $[Bu_3NH]^+$ as counterion.

To study the potential of $[SnCB_{10}H_{11}]^-$ as a ligand in transition metal chemistry and inspired by the various reactions of $[SnB_{11}H_{11}]^{2-}$ with gold electrophiles,[13,14] we started our investigations with the reaction of $[Bu_4N][SnCB_{10}H_{11}]$ with $[Au(PPh_3)Cl]$.

The isoelectronic stannaborate $[SnB_{11}H_{11}]^{2-}$ reacts with $[Au(PPh_3)Cl]$ in dichloromethane at room temperature within 1 h to form tin-bridged gold dimers (vide infra),[13] whereas with the new carbastannaborate no reaction could be detected. At elevated temperature (CH_2Cl_2 under reflux) a change in color from colorless to yellow was observed within 48 h (eq 2). Instead of forming a gold dimer, a tetranuclear gold cluster $[Au_4(PPh_3)_4(SnCB_{10}H_{11})_2]$, **2**, was isolated. This surprising mixed-valence gold coordination compound is the product of a redox reaction. However, the reducing agent is so far unknown to us.

Exploring the behavior of the cluster $[SnCB_{10}H_{11}]^-$, **1**, toward rhodium, the addition of $[Bu_4N]$·**1** to a solution of Wilkinson's catalyst, $[Rh(PPh_3)_3Cl]$, in dichloromethane led immediately to a change in color from orange-brown to blood-red (eq 3).

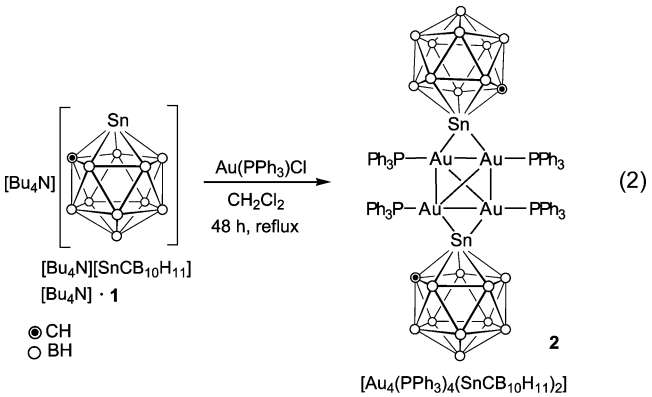

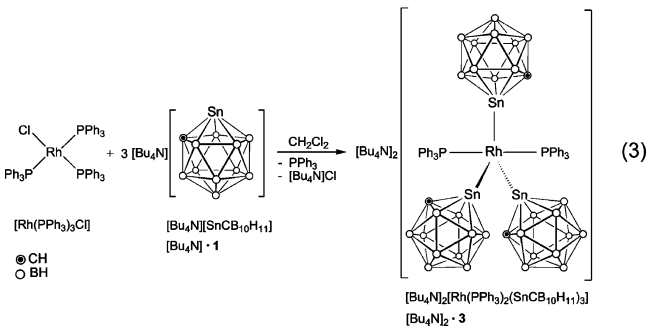

From this solution the pentacoordinated rhodium complex $[Bu_4N]_2[Rh(PPh_3)_2(SnCB_{10}H_{11})_3]$, $[Bu_4N]_2$·**3**, was isolated. Reacting the starting materials in a 1:3 ratio yielded the rhodium complex **3** almost quantitatively on the basis of NMR spectroscopy. The 3-fold carbastannaborate coordination compound is the only detected product even in 1:1 and 1:2 reaction mixtures between *closo*-cluster **1** and the rhodium electrophile deduced from NMR spectroscopical investigations.

Solid-State Structures. Crystals suitable for single-crystal structure analysis of the carbastanna-*closo*-dodecaborate salt were obtained by slow diffusion of hexane into a dichloromethane solution of $[Bu_3NH]$·**1** and $[Bu_3NH]Cl$. $[Bu_3NH]$·**1** cocrystallizes with 1 equiv of $[Bu_3NH]Cl$, yielding colorless crystals. The molecular structure of the anion of $[Bu_3NH][SnCB_{10}H_{11}]$ with selected interatomic distances is depicted in Figure 2. The tin vertex is centered above the five-membered face consisting of four BH units (B3, B6, B7, B11) and one CH unit (C1). The carbon atom inside the cluster can be assigned unambiguously: The boron−carbon bonds are with 1.704(7) and 1.718(7) Å (C1−B6, C1−B3) shorter than the boron−boron distances, at 1.828(8), 1.832(8), and 1.805(8) Å (B3−B7, B7−B11, B11−B6), and the tin−carbon distance of 2.466(5) Å is the longest distance between the atoms of the pentagonal face and the tin atom. Furthermore, the position of the carbon atom is also confirmed by a minimization of the wR_2 value. The cage carbon atoms in the crystal structures of **2** and $[Bu_4N]_2$·**3** were determined analogously. The tin−boron distances range from 2.360(5) to 2.436(5) Å and are, on average, a little longer than the tin−boron distances in $[SnB_{11}H_{11}]^{2-}$ [2.382(4)−2.389(3) Å].[6,15]

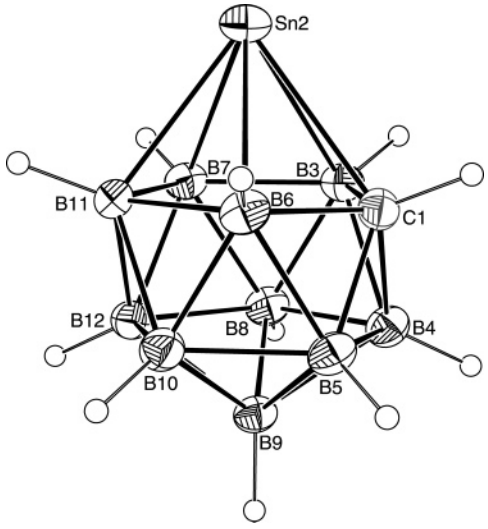

Figure 2. ORTEP plot (30% probability level) of the molecular structure of $[SnCB_{10}H_{11}]^-$, **1**. The cation and the cocrystallized $[Bu_3NH]Cl$ have been omitted for clarity. Selected bond distances [Å]: Sn2−C1 2.466(5), Sn2−B3 2.384(6), Sn2−B6 2.436(5), Sn2−B7 2.360(5), Sn2−B11 2.400(5).

Orange crystals of **2** were obtained by slow diffusion of hexane into a solution of the gold cluster **2** in dichloromethane. The structure refinement reveals that the asymmetric unit consists of two molecules of $[Au_4(PPh_3)_4(SnCB_{10}H_{11})_2]$, **2**, and five CH_2Cl_2 solvate molecules. In Figure 3 the molecular structure of one of these two complexes is shown, and selected interatomic angles and distances are summarized in Table 2.

Complex **2** consists of a Au_4 skeleton with two opposite edges bridged by μ_2-coordinated heteroborates $[SnCB_{10}H_{11}]^-$. These two bridged Au−Au contacts are significantly shorter than the nonbridged ones. This structural motif is already known from $[Au_4(PPh_3)_4(SnCl_3)_2]$ and $[Au_4(PPh_3)_4I_2]$, where two edges of the gold tetrahedron are bridged by $SnCl_3^-$ and I^-, respectively.[16−18] The Au−Au distances of the tin-bridged edges

(13) Hagen, S.; Pantenburg, I.; Weigend, F.; Wickleder, C.; Wesemann, L. *Angew. Chem., Int. Ed.* **2003**, *42*, 1501−1505.
(14) Hagen, S.; Wesemann, L.; Pantenburg, I. *Chem. Commun.* **2005**, 1013−1015.
(15) Gädt, T.; Wesemann, L. *Z. Anorg. Allg. Chem.* **2007**, *633*, 693−699.
(16) *Gold*; Schmidbaur, H., Ed.; Wiley: Chichester, U.K., 1999.
(17) Mingos, D. M. P.; Powell, H. R.; Stolberg, T. L. *Transition Met. Chem.* **1992**, *17*, 334−337.
(18) Demartin, F.; Manassero, M.; Naldini, L.; Ruggeri, R.; Sansoni, M. *J. Chem. Soc., Chem. Commun.* **1981**, 222−223.

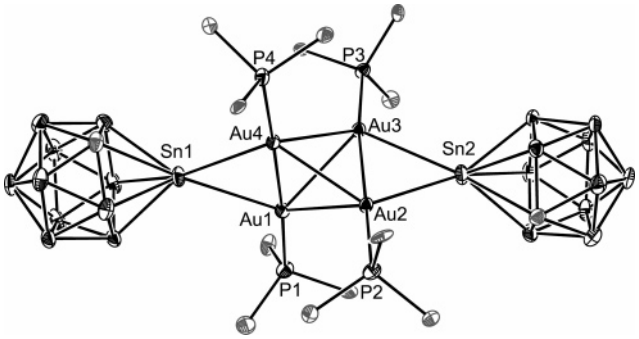

Figure 3. ORTEP plot (30% probability level) of the molecular structure of $[Au_4(PPh_3)_4(SnCB_{10}H_{11})_2]$, **2**. The second complex, which is contained in the asymmetric unit, the solvent molecules, and H atoms have been omitted, and phenyl rings are symbolized by the *ipso* C for clarity. Selected bond distances and angles of this selected complex are summarized in Table 1.

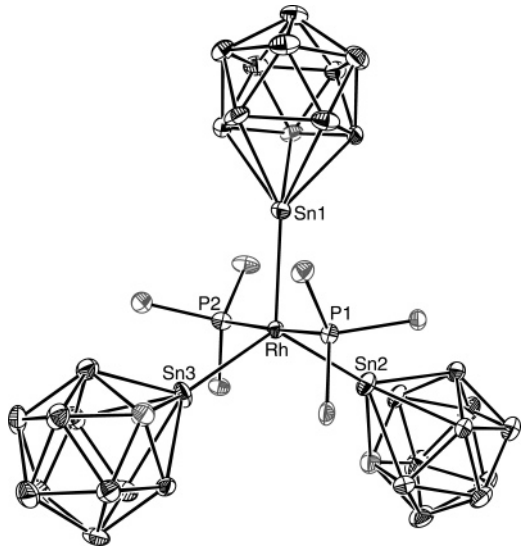

Figure 4. ORTEP plot (30% probability level) of the molecular structure of $[Rh(PPh_3)_2(SnCB_{10}H_{11})_3]^{2-}$, **3**. H atoms and cations have been omitted and phenyl rings are symbolized by the *ipso* C for clarity. Selected bond distances [Å] and angles [deg]: Rh−Sn1 2.5644(5), Rh−Sn2 2.5829(5), Rh−Sn3 2.5662(5), Rh−P1 2.345(1), Rh−P2 2.337(1), P1−Rh−P2 175.90(5), Sn1−Rh−Sn2 117.26(2), Sn1−Rh−Sn3 122.65(2), Sn2−Rh−Sn3 120.06(2), P1−Rh−Sn1 87.41(3), P1−Rh−Sn2 89.87(3), P1−Rh−Sn3 90.81(3), P2−Rh−Sn1 90.08(3), P2−Rh−Sn2 94.16(3), P2−Rh−Sn3 87.82(3).

ranging from 2.5993(8) to 2.6150(9) Å are a little shorter than the related Au−Au bonds in $[Au_4(PPh_3)_4(SnCl_3)_2]$, which start at 2.6341(5) Å,[17] and correspond to the Au−Au distances in $[Au_2(PPh_3)_2(SnB_{11}H_{11})_2]^{2-}$ [2.590(1)−2.625(1) Å].[13] Further distances and angles are compared in Table 2.

The bridging of two opposite edges of the gold cluster by the tin(II) compound **1** results in a distorted tetrahedron reflected in variations of the Au−Au−Au bond angles. The tin-bridged P−Au−Au−P axes are close to linearity, which is expected for $[Au_4(PPh_3)_4]^{2+}$-containing compounds.[19] Small deviations from 180° of the Au−Au−P bond angles, which are observable in each of the three compounds listed in Table 2, may be attributed to steric effects. With an average value of 2.816 Å the Au−Sn distances in **2** are counted among the long Au−Sn bond lengths, which range from 2.565(1) to 2.973(8) Å.[17,20−24]

Table 1. Selected Bond Distances [Å] and Angles [deg] for One of the Two $[Au(PPh_3)_4(SnCB_{10}H_{11})_2]$, 2, Complexes in the Asymmetric Unit

atoms	distance	atoms	distance
	Distances for the Metal Cage		
Au1−Au2	2.8170(9)	Au2−Au3	2.5993(8)
Au1−Au3	2.8467(9)	Au2−Au4	2.7799(9)
Au1−Au4	2.6058(8)	Au3−Au4	2.8611(9)
	Metal−Ligand Distances		
Au1−Sn1	2.891(1)	Au1−P1	2.298(4)
Au2−Sn2	2.727(1)	Au2−P2	2.299(4)
Au3−Sn2	2.936(1)	Au3−P3	2.297(4)
Au4−Sn1	2.757(1)	Au4−P4	2.310(4)
atoms	**angle**	**atoms**	**angle**
	Angles for the Metal Cage		
Au1−Au2−Au3	63.27(2)	Au2−Au1−Au3	54.63(2)
Au1−Au2−Au4	55.49(2)	Au2−Au1−Au4	61.53(2)
Au1−Au3−Au2	62.10(2)	Au2−Au3−Au4	60.99(2)
Au1−Au3−Au4	54.33(2)	Au2−Au4−Au3	54.85(2)
Au1−Au4−Au2	62.98(2)	Au3−Au1−Au4	63.12(2)
Au1−Au4−Au3	62.56(2)	Au3−Au2−Au4	64.16(2)
	Metal−Ligand Angles		
Au4−Sn1−Au1	54.89(3)	Au2−Sn2−Au3	54.49(3)
P1−Au1−Au2	120.0(1)	P3−Au3−Au1	121.7(1)
P1−Au1−Au3	121.1(1)	P3−Au3−Au2	172.8(1)
P1−Au1−Au4	175.8(1)	P3−Au3−Au4	126.2(1)
P2−Au2−Au1	118.5(1)	P4−Au4−Au1	178.7(1)
P2−Au2−Au3	175.7(1)	P4−Au4−Au2	118.3(1)
P2−Au2−Au4	113.2(1)	P4−Au4−Au3	118.5(1)

Red, needle-shaped single crystals suitable for single-crystal structure analysis of $[Bu_4N]_2$·**3** were grown by slow diffusion of hexane into a solution of $[Bu_4N]_2[Rh(PPh_3)_2(SnCB_{10}H_{11})_3]$ in CH_2Cl_2. In Figure 4 the molecular structure of **3** is depicted together with selected interatomic angles and distances. The two triphenyl phosphine ligands occupy the axial positions of a trigonal bipyramid, while the three tin-containing ligands are placed in equatorial positions. This structure has also been postulated for $[Rh(CNcy)_2(SnCl_3)_3]^{2-}$, where the authors argue that the stronger σ-donor CNcy (cyclohexyl isonitrile) prefers the axial positions and the weak σ-donor and π-acceptor $[SnCl_3]^-$ occupies the equatorial positions.[25]

The Rh−Sn bond distances for **3**, at 2.5644(5) Å (Rh−Sn1), 2.5829(5) Å (Rh−Sn2), and 2.5662(5) Å (Rh−Sn3), are situated at the lower limit of known Rh−Sn bond lengths, which range from 2.526(1) Å in $Rh[Sn(N^tBu)_2SiMe_2]_5Cl$ to 2.651(2) Å in $[Rh(SnCl_3)(NBD)(dppb)]$ (NBD = norbornadiene, dppb = 1,4-bis(diphenylphosphino)butane).[26−38] A similar value is found

(19) Evans, D. G.; Mingos, D. M. P. *J. Organomet. Chem.* **1982**, *232*, 171−191.
(20) Demidowicz, Z.; Johnston, R. L.; Machell, J. C.; Mingos, D. M. P.; Williams, I. D. *J. Chem. Soc., Dalton Trans.* **1988**, 1751−1756.
(21) Clegg, W. *Acta Crystallogr., Sect. B* **1978**, *B34*, 278−281.
(22) Gade, L. H. *Eur. J. Inorg. Chem.* **2002**, 1257−1268.
(23) Contel, M.; Hellmann, K. W.; Gade, L. H.; Scowen, I. J.; McPartlin, M.; Laguna, M. *Inorg. Chem.* **1996**, *35*, 3713−3715.
(24) Findeis, B.; Contel, M.; Gade, L. H.; Laguna, M.; Gimeno, M. C.; Scowen, I. J.; McPartlin, M. *Inorg. Chem.* **1997**, *36*, 2386−2390.
(25) Kretschmer, M.; Pregosin, P. S.; Rüegger, H. *J. Organomet. Chem.* **1983**, *241*, 87−98.
(26) Veith, M.; Stahl, L.; Huch, V. *Inorg. Chem.* **1989**, *28*, 3278−3280.
(27) Garcia, V.; Garralda, M. A.; Pinilla, E. *J. Organomet. Chem.* **1997**, *545−546*, 93−98.
(28) Garcia, V.; Garralda, M. A.; Hernandez, R.; Monge, M. A.; Pinilla, E. *J. Organomet. Chem.* **1994**, *476*, 41−46.
(29) Circu, V.; Fernandes, M. A.; Carlton, L. *Inorg. Chem.* **2002**, *41*, 3859−3865.
(30) Bott, S. G.; Machell, J. C.; Mingos, D. M. P.; Watson, M. J. *J. Chem. Soc., Dalton Trans.* **1991**, 859−862.
(31) Bikrani, M.; Garralda, M. A.; Ibarlucea, L.; Pinilla, E. *J. Organomet. Chem.* **1995**, *489*, 93−99.
(32) Garralda, M. A.; Pinilla, E.; Monge, M. A. *J. Organomet. Chem.* **1992**, *427*, 193−200.

Table 2. Comparison of Distances and Angles of Three Tin-Bridged Gold Complexes

	$[Au_4(PPh_3)_4(SnCB_{10}H_{11})_2]$	$[Au_2(PPh_3)_2(SnB_{11}H_{11})_2]^{2-}$	$[Au_4(PPh_3)_4(SnCl_3)_2]$
Au−Au bond lengths [Å]	2.5993(8)−2.8588(9)	2.625(1)	2.6341(5)−2.8128(5)
Au−Au−Au bond angles [deg]	54.33(2)−64.16(2)		56.34(1)−62.72(1)
Au−Au−P bond angles [deg]	170.7(1)−178.7(1)	178.78(4)	175.16(6)−177.34(6)
Au−Sn bond lengths [Å]	2.727(1)−2.936(1)	2.737(1)−2.761(1)	2.8150(7)−2.9725(8)
Au−Sn−Au bond angles [deg]	54.49(3)−55.63(3)	57.03(1)	54.06(1)
ref	present work	13	17

in coordination compound [Rh(bipy′)(Cp*)($SnB_{11}H_{11}$)] (bipy′ = 4,4′-di-*tert*-butyl-2,2′-bipyridine, Cp* = pentamethylcyclopentadiene),[39] which includes also a tin-containing icosahedral boron cluster molecule, $[SnB_{11}H_{11}]^{2-}$: Rh−Sn = 2.578(1) Å. Complex **3** adopts nearly perfect trigonal bipyramidal symmetry with negligible distortion, which is reflected in the axial bond angle of P1−Rh−P2, which is close to linearity at 175.90(5)°, the in-plane bond angles Sn−Rh−Sn, with an average value of 119.99°, and the P−Rh−Sn angles between the perpendicular axis and the plane, with an average value of 90.03°.

NMR Spectroscopy. The observed six signals in the $^{11}B\{^1H\}$ NMR spectrum with an intensity ratio of 1:1:2:2:2:2 reflect the C_s symmetry of **1**. The signals at −6.0, −7.1, −8.3, −10.5, −14.6, and −15.3 ppm in the $^{11}B\{^1H\}$ NMR spectrum can be correlated to the respective proton signals in the ^1H NMR spectrum at 2.20, 3.53, 0.99, 2.11, 2.04, and 1.38 ppm by an $^{11}B\{^1H\}-^1H$ HETCOR NMR experiment, and the boron−hydrogen coupling constants between 122 and 158 Hz are in the normal range.[40] $^{11}B\{^1H\}-^{11}B\{^1H\}$ COSY (Figure 5) and $^{11}B\{^1H\}-^{11}B\{^1H\}$ TOCSY NMR experiments allow a definite assignment of the two signals at −10.5 (B8, B10) and −15.3 ppm (B3, B6) only. The $^{119}Sn\{^1H\}$ NMR spectrum shows a broad signal at −495 ppm with a line width of 868 Hz, and the $^{13}C\{^1H\}$ NMR spectrum shows a very small and broad signal at 51.8 ppm, which can be assigned to the carbon atom of the cluster. Recording a $^1H\{^{13}C\}$ GRASP HSQC NMR spectrum, the signal of the attached proton could be identified at 1.76 ppm.

Compared to **1**, the range of chemical shifts in the $^{11}B\{^1H\}$ NMR spectrum, which shows four broad signals at −6.1, −9.3, −11.0, and −15.2 ppm with an intensity ratio of 2:2:4:2, and in the $^{119}Sn\{^1H\}$ NMR spectrum of **2**, with a single signal at −492 ppm, remains unchanged apart from a very small deviation. However, the $^{31}P\{^1H\}$ NMR experiment exhibits a broad signal at 61.5 ppm, which is remarkably displaced against the chemical shift of the educt (33.2 ppm) but similar to the $^{31}P\{^1H\}$ NMR shift of $[Au_4(PPh_3)_4(SnCl_3)_2]$ of 56.9 ppm.[17]

In contrast to the $[SnB_{11}H_{11}]^{2-}$-bridged gold dimers and trimers,[13] we were not able to observe a phosphorus−tin coupling at room temperature. In order to eventually freeze dynamics in solution, which could inhibit the observation of the coupling and cause the broadening, the sample was cooled to −78 °C, but still no phosphorus−tin coupling was observed. In the case of $[Au_4(PPh_3)_4(SnCl_3)_2]$, Mingos et al. did not report this coupling because the low signal-to-noise ratio of their $^{31}P\{^1H\}$ NMR spectrum prevented any conclusions.[17] Therefore, no example in the literature is known to us where a phosphorus−tin coupling for an Au_4 complex is reported. Furthermore, $[Au_4(P^tBu_3)_4](BF_4)_2$ is an example[41] of a tetrahedral gold cluster without any bridging group or atom, suggesting that **2** dissociates in solution into $[Au_4(PPh_3)_4]^{2+}$ and 2 $[SnCB_{10}H_{11}]^-$. This could be an evident explanation for the missing phosphorus−tin coupling even at low temperature and only small changes in the $^{119}Sn\{^1H\}$ and $^{11}B\{^1H\}$NMR spectrum.

Observable in the $^{119}Sn\{^1H\}$ NMR spectrum of **3** is one signal at − 276 ppm, which shows tin−tin coupling ($^2J_{^{119}Sn,^{117}Sn}$ = 6400 Hz) and tin−rhodium coupling ($^1J_{^{119}Sn,^{103}Rh}$ = 760 Hz). The tin−phosphorus coupling is not resolved in this spectrum due to the large line width of the signal, which may be attributed to additional tin−boron coupling. However, the tin−phosphorus coupling ($^2J_{^{117/119}Sn,^{31}P}$ = 313 Hz) can be determined from the signal at 36.4 ppm in the $^{31}P\{^1H\}$ NMR spectrum. Additionally, rhodium−phosphorus coupling ($^1J_{^{103}Rh,^{31}P}$ = 88 Hz) is detected. The $^{11}B\{^1H\}$ NMR spectrum consists of a small broad signal assigned to the boron atom, which is situated antipodal to the tin atom, while the remaining resonances collapse to one large signal because of fortuitous isochronism. This phenomenon is already known from $[SnB_{11}H_{11}]^{2-}$ in complexes with transition metals.[15]

^{119}Sn Mössbauer Spectroscopy. The ^{119}Sn Mössbauer spectrum of $[MePPh_3][SnCB_{10}H_{11}]$, $[MePPh_3]$·**1**, recorded at 78 K together with a transmission integral fit is depicted in Figure 6. The spectrum was fitted by a single tin site at an isomer shift (IS) of 2.90(1) mm·s^{-1} with an experimental line width of 0.92(2) mm·s^{-1} and a quadrupole splitting of 2.33(1) mm·s^{-1}.

It has been suggested that the isomer shift in the ^{119}Sn Mössbauer spectra is proportional to variation of the 5s electron density.[42] The decrease in positive shift toward α-tin (sp^3 configuration, IS = 2.05 mm·s^{-1}) in a series of tin(II) materials is likely to be proportional to an increasing loss of effective 5s density in the hypothetical $5s^2$ Sn^{2+} ion. Compounds with IS values close to α-tin seem to exhibit a mostly covalent bonding situation, while higher IS values are associated with a more ionic bonding character.

The increasing isomer shift in the series shown in Table 3 can be thus interpreted as an indicator of the tin−cage interaction, which seems rather covalent in $[SnB_{11}H_{11}]^{2-}$ and rather ionic in $[SnC_2B_9H_{11}]$. The value for **1** is comparable to the IS shift of the stanna-*closo*-dodecaborate, $[SnB_{11}H_{11}]^{2-}$, and could therefore be classified among the more covalent species. This behavior is even more pronounced in intermetallic compounds with covalently bonded polyanions. To give an example, for the three-dimensional $[PdSn_2]$ and $[AuSn_2]$ polyanions of $Ca[PdSn_2]$[37] and $Li_2[AuSn_2]$[44] one observes isomer shifts of 2.21(3) and 2.15(2) mm·s^{-1}, respectively. The course of these

(33) Werner, H.; Gevert, O.; Haquette, P. *Organometallics* **1997**, *16*, 803−806.
(34) Chan, D. M. T.; Marder, T. B. *Angew. Chem., Int. Ed. Engl.* **1988**, *100*, 442−443.
(35) Mezailles, N.; Rosa, P.; Ricard, L.; Mathey, F.; Le Floch, P. *Organometallics* **2000**, *19*, 2941−2943.
(36) Niepmann, D.; Pöttgen, R.; Künnen, B.; Kotzyba, G.; Rosenhahn, C.; Mosel, B. D. *Chem. Mater.* **1999**, *11*, 1597−1602.
(37) Hoffmann, R.-D.; Kussmann, D.; Rodewald, U. C.; Pöttgen, R.; Rosenhahn, C.; Mosel, B. D. *Z. Naturforsch.* **1999**, *54*, 709−717.
(38) Schmidt, T.; Johrendt, D.; Sebastian, C. P.; Pöttgen, R.; Łątka, K.; Kmieć, R. *Z. Naturforsch.* **2005**, *60*, 1036−1042.
(39) Marx, T.; Wesemann, L.; Dehnen, S. *Z. Anorg. Allg. Chem.* **2001**, *627*, 1146−1150.
(40) Heřmánek, S. *Chem. Rev.* **1992**, *92*, 325−362.
(41) Zeller, E.; Beruda, H.; Schmidbaur, H. *Inorg. Chem.* **1993**, *32*, 3203−3204.
(42) Donaldson, J. D.; Senior, B. J. *J. Chem. Soc.* **1966**, 1798−1800.
(43) Marx, T.; Mosel, B.; Pantenburg, I.; Hagen, S.; Schulze, H.; Wesemann, L. *Chem.−Eur. J.* **2003**, *9*, 4472−4478.
(44) Wu, Z.; Mosel, B. D.; Eckert, H.; Hoffmann, R.-D.; Pöttgen, R. *Chem.−Eur. J.* **2004**, *10*, 1558−1564.

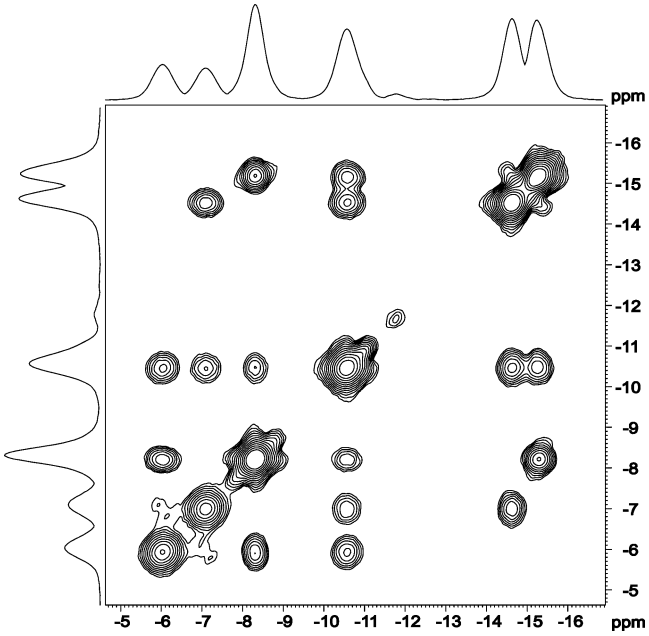

Figure 5. $^{11}B\{^1H\}-^{11}B\{^1H\}$ COSY NMR spectrum of $[Bu_4N][SnCB_{10}H_{11}]$, $[Bu_4N]$·**1**, in CD_2Cl_2 with signals at −6.0, −7.1, −8.3, −10.5 (B8, B10), −14.6 and −15.3 ppm (B3, B6).

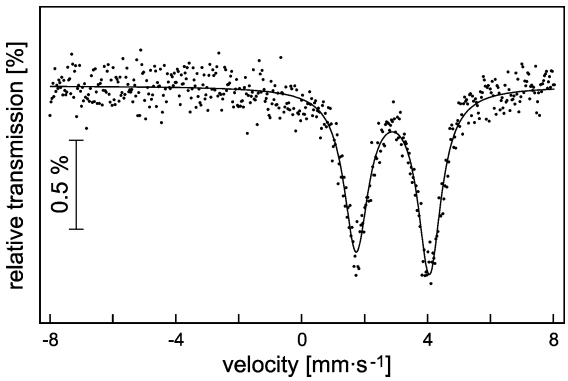

Figure 6. Experimental ^{119}Sn Mössbauer spectrum at 78 K of $[MePPh_3][SnCB_{10}H_{11}]$, $[MePPh_3]$·**1**, with a transmission integral fit (solid line).

Table 3. Isomer Shifts (IS) and Electric Quadrupole Splitting (ΔE_Q) from ^{119}Sn Mössbauer Data for Icosahedral Boron Cage Compounds[a]

compound	IS/mm·s^{-1}	ΔE_Q/mm·s^{-1}	ref
$[Bu_3NMe]_2[SnB_{11}H_{11}]$	2.46	1.71	43
$[MePPh_3][SnCB_{10}H_{11}]$	2.90(1)	2.33(1)	present work
$[SnC_2B_9H_{11}]$	4.67(4)	3.83(4)	11

[a] Numbers in parentheses represent the statistical error in the last digit.

isomer shifts directly correlates with the s electron density at the tin nuclei.[45]

The quadrupole splitting observed in the Mössbauer spectra of tin(II) compounds is related to the asymmetry of the environment of the tin atom and is caused by the interaction between the nuclear quadrupole moment and inhomogeneous electric field gradients in the material: the more asymmetric the environment of the tin atom, the larger the quadrupole splitting, as can be seen in Table 3. The quadrupole splitting of **1** (C_s) of 2.33(1) mm·s^{-1} reflects the lower site symmetry compared to $[SnB_{11}H_{11}]^{2-}$(C_{5v}) at 1.71 mm·s^{-1}.

(45) Lippens, P. E. *Phys. Rev.* **1999**, *60*, 4576−4586.

Conclusion. With $[SnCB_{10}H_{11}]^-$ we have characterized a novel heteroborate that is easily synthesized on a large scale and easy to handle due to its stability against air and moisture. Our first investigations of the chemistry of this carbastannaborate proved the cluster to be nucleophilic at the tin site but lower in reactivity than its isolobal compound $[SnB_{11}H_{11}]^{2-}$. Electrophilic behavior, like its other isolobal cluster $[SnC_2B_9H_{11}]$ shows, was so far not observed.

Experimental Section

General Methods. All manipulations were carried out under dry argon in Schlenk glassware; solvents were dried and purified by standard methods and stored under argon. Elemental analyses were performed by the Institut für Anorganische Chemie, Universität Tübingen, using a Vario EL analyzer. All chemicals were purchased commercially except $[Me_3NH][CB_{10}H_{13}]$, which was prepared according to slightly modified literature methods by the reduction of $Me_3NCB_{10}H_{13}$ with sodium metal.[12]

NMR Spectroscopy. ^{11}B, ^{31}P, and ^{119}Sn NMR spectra were obtained using a Bruker DRX-250 NMR spectrometer equipped with a 5 mm ATM probe head and operating at 80.25 (^{11}B), 101.25 (^{31}P), and 93.25 MHz (^{119}Sn). ^1H, ^{13}C, ^{11}B, and the 2D NMR experiments were performed using a Bruker Avance II + 500 NMR spectrometer equipped with a 5 mm TBO probe head and operating at 500.13 (^1H), 125.76 (^{13}C), and 160.46 MHz (^{11}B). Chemical shifts are reported in δ values relative to external TMS (^1H, ^{13}C), BF_3·Et_2O (^{11}B), 85% H_3PO_4 (aq) (^{31}P), or $SnMe_4$ (^{119}Sn) using the chemical shift of the respective solvent ^2H resonance frequency.

Preparation of $[MePPh_3][SnCB_{10}H_{11}]$, $[MePPh_3]$·1. A solution of $[Me_3NH][CB_{10}H_{13}]$ (703 mg, 3.6 mmol) in THF (40 mL) was cooled to −78 °C, and *n*-butyllithium (4.5 mL, 2.5 M in hexane) was slowly added. The mixture was stirred for 3 h at room temperature, and a white precipitate was formed. When butane evolution had stopped, the suspension was again cooled to −78 °C and a solution of $SnCl_2$ (885.8 mg, 4.69 mmol) in THF (6 mL) was added. Stirring the mixture for 12 h at room temperature caused the precipitate to disappear and a yellow-brown solution was formed. After removing the solvent in vacuo the residue was dissolved in water (20 mL) and filtered into a solution of $[MePPh_3]$-Br (1.5 g, 4.2 mmol) in water (10 mL). The formed colorless suspension was allowed to cool overnight in a refrigerator to precipitate $[MePPh_3][SnCB_{10}H_{11}]$, which was collected via filtration, washed with cold water and diethyl ether, and dried in vacuo. Yield: 1.81 g, 95%. $^{11}B\{^1H\}$ NMR (CD_2Cl_2): δ −6.0 (1B), −7.1 (1B), −8.3 (2B), −10.5 (B8, B10), −14.6 (2B), −15.3 ppm (B3, B6). ^1H NMR (CD_2Cl_2): δ 0.99 (SnCH(B*H*)$_{10}$, 2H), 1.38 (SnCH-(B*H*)$_{10}$, H3, H6), 1.76 (SnC*H*(BH)$_{10}$), 2.04 (SnCH(B*H*)$_{10}$, 2H), 2.11 (SnCH(B*H*)$_{10}$, H8, H10), 2.20 (SnCH(B*H*)$_{10}$, 1H), 3.53 ppm (SnCH-(B*H*)$_{10}$, 1H). $^{13}C\{^1H\}$ NMR (CD_2Cl_2): δ 51.8 ppm (Sn*C*B$_{10}$H$_{11}$). $^{119}Sn\{^1H\}$ NMR (CD_2Cl_2): δ −495 ppm. fwhh: 868 Hz. Anal. Calcd (%) for $[MePPh_3][SnCB_{10}H_{11}]$·$0.5CH_2Cl_2$: C 43.22, H 5.31. Found: C 43.42, H 5.30.

$[Bu_4N]$·**1** and $[Bu_3NH]$·**1** were synthesized analogously but using different counterions. Single crystals of $[Bu_3NH]$·**1** suitable for X-ray analysis were grown by layering a solution of $[Bu_3NH]$·**1** and $[Bu_3NH]Cl$ in CH_2Cl_2 with hexane.

Preparation of $[Au_4(PPh_3)_4(SnCB_{10}H_{11})_2]$, 2. To a stirred solution of $[Bu_4N]$·**1** (210 mg, 0.44 mmol) in CH_2Cl_2 (40 mL) was added solid $[Au(PPh_3)Cl]$ (551 mg, 1.11 mmol). The mixture was refluxed for 48 h, and a deep yellow solution was formed. Single crystals suitable for X-ray analysis were grown by layering this reaction mixture with hexane. Yield: 39 mg, 8%. $^{11}B\{^1H\}$ NMR (CD_2Cl_2): δ −6.1 (2B), −9.3 (2B), −11.0 (4B), −15.2 ppm (2B). $^{31}P\{^1H\}$ NMR (CD_2Cl_2): δ 61.5 ppm. $^{119}Sn\{^1H\}$ NMR (CD_2Cl_2): δ −492 ppm. fwhh: 1548 Hz. Anal. Calcd (%) for $Au_4Sn_2P_4B_{20}C_{74}H_{82}$: C 38.03, H 3.54. Found: C 37.37, H 3.47.

Table 4. Crystal Data and Refinement Parameters for Compounds [Bu_3NH]·1, 2, and [Bu_4N]·3

empirical formula	$C_{25}H_{67}B_{10}ClN_2Sn$	$C_{76}H_{87}B_{20}Cl_4P_4Sn_2Au_4$	$C_{72}H_{137}B_{30}Cl_2N_2P_2RhSn_3$
fw	658.05	2507.58	1946.96
temperature [K]	173(2)	173(2)	173(2)
space group	$P2_1/c$	$P2_1/n$	$P2_1/c$
a [Å]	10.173(1)	25.188(2)	17.6722(8)
b [Å]	11.5674(7)	20.2044(9)	22.5290(7)
c [Å]	31.877(3)	35.831(2)	24.228(1)
β [deg]	95.862(9)	101.118(5)	99.158(3)
volume [Å^3]	3731.5(6)	17893(2)	9523.2(7)
Z	4	8	4
calcd density [g·cm^{-1}]	1.17	1.86	1.36
absorp coeff [cm^{-1}]	0.08	0.73	0.11
final indices[a,b] [$I > 2\sigma(I)$]	$R_1 = 0.0607$	$R_1 = 0.0788$	$R_1 = 0.0572$
	$wR_2 = 0.1292$	$wR_2 = 0.1068$	$wR_2 = 0.0972$
indices (all data)	$R_1 = 0.0894$	$R_1 = 0.1663$	$R_1 = 0.0895$
	$wR_2 = 0.1417$	$wR_2 = 0.1256$	$wR_2 = 0.1075$

[a] $R_1 = \sum||F_o| - |F_c||/\sum|F_o|$. [b] $wR_2 = (\sum w(|F_o| - |F_c|)^2/\sum w|F_o|^2)^{1/2}$.

Preparation of [Bu_4N]$_2$[Rh(PPh_3)$_2$($SnCB_{10}H_{11}$)$_3$], [Bu_4N]·3. Solid [Bu_4N]·**1** (53 mg, 0.11 mmol) was added to a solution of [Rh(PPh_3)$_3$Cl] (34 mg, 0.037 mmol) in CH_2Cl_2 (10 mL). The solution became red immediately. After removing all volatiles in vacuo the crude product was washed with hexane (3 × 10 mL) and dried in vacuo. Long, red, needle-shape single crystals suitable for X-ray analysis were grown by slow diffusion of hexane into a solution of the crude product in dichloromethane. Yield: 37 mg, 53%. $^{11}B\{^1H\}$ NMR (CD_2Cl_2): δ −7.7 (1B), −10.0 to −17.0 ppm (9B). $^{31}P\{^1H\}$ NMR (CD_2Cl_2): δ 36.4 ppm (2P, $^1J_{^{103}Rh,^{31}P} = 88$ Hz, $^2J_{^{117/119}Sn,^{31}P} = 313$ Hz). $^{119}Sn\{^1H\}$ NMR (CD_2Cl_2): δ −276 ppm ($^1J_{^{119}Sn,^{103}Rh} = 760$ Hz, $^2J_{^{119}Sn,^{117}Sn} = 6400$ Hz). Anal. Calcd (%) for $RhSn_3P_2N_2B_{30}C_{71}H_{135}$: C 45.79, H 7.31, N 1.5. Found: C 45.64, H 6.06, N 1.33.

X-ray Structure Determination. X-ray data for compounds [Bu_3NH]·**1**, **2**, and [Bu_4N]·**3** were collected on a Stoe IPDS 2T and were corrected for Lorentz and polarization effects and absorption by air. Numerical absorption correction based on crystal-shape optimization was applied for all data except compound [Bu_3-NH]·**1**. The program Stoe X-Area including X-Red and X-Shape was used for data reduction and absorption correction, and the WinGX suite of programs including SHELXS-97[46] and SHELXL-97[47] was used for structure solution and refinement. Crystal data and refinement parameters are listed in Table 4.

[Bu_3NH][$SnCB_{10}H_{11}$]·[Bu_3NH]Cl. The cluster [Bu_3NH]·**1** co-crystallized together with 1 equiv of [Bu_3NH]Cl in the asymmetric unit. One of the butyl chains including C210−C212 showed disorder with occupancies of 74.2:25.8, and DFIX, DANG, and EADP restraints were applied. All hydrogen atoms were placed in calculated positions and refined with isotropic displacement parameters.

2[Au_4(PPh_3)$_4$($SnCB_{10}H_{11}$)$_2$]·5CH_2Cl_2. There are two independent gold complexes **2** and five solvent molecules in the asymmetric unit. The occupancy factor of 2 dichloromethane molecules including C40, Cl41, Cl42 and C50, Cl51, Cl52 was set to 0.5 due to spatial disorder. These two molecules were refined with isotropic displacement parameters, and DFIX restraints were applied for all carbon−chlorine interatomic distances. All hydrogen atoms were kept at calculated positions.

[Bu_4N]$_2$[Rh(PPh_3)$_2$($SnCB_{10}H_{11}$)$_3$]·CH_2Cl_2. The complex [Bu_4N]·**3** crystallized together with 1 equiv of solvent, which is distributed over two equivalent positions. One of the cluster ligands, including the atoms C1 and B10−B19, showed spatial disorder with occupancies of 82:18. The cluster belonging to Sn1 is slightly tilted against the Rh−Sn1 axis and ca. 35° rotated around the axis through Sn1 and the antipodal boron atom. The four butyl chains including the carbon atoms C40−C56 of one cation are spatially disordered as well with occupancies of 53:47, while for the second cation only a spatial disorder for the terminal C31 occurs with occupancies of 46:54. All hydrogen atoms were placed in calculated positions and refined with isotropic displacement parameters.

^{119}Sn Mössbauer Spectroscopy. A $Ca^{119}SnO_3$ source was available for the ^{119}Sn Mössbauer spectroscopic investigations. The sample was placed within a thin-walled glass container at a density of about 10 mg Sn·cm^{-2}. A palladium foil of 0.05 mm thickness was used to reduce the Sn_K X-rays concurrently emitted by this source. The measurement was conducted in the usual transmission geometry at 78 K.

Acknowledgment. This work was supported by the Deutsche Forschungsgemeinschaft.

Supporting Information Available: This material is available free of charge via the Internet at http://pubs.acs.org.

OM7006858

(46) Sheldrick, G. M. *SHELXS-97, Program for the Solution of Crystal Structures*; University of Göttingen, 1997.

(47) Sheldrick, G. M. *SHELXL-97 Program for Crystal Stucture Refinement*; University of Göttingen, 1997.